Accuracy Quantification and Improvement of Serial Micropositioning Robots for In-Plane Motions

Ning Tan, *Member, IEEE*, Cédric Clévy, *Member, IEEE*, Guillaume J. Laurent, *Member, IEEE*, Patrick Sandoz, and Nicolas Chaillet, *Member, IEEE*

***Abstract*—High positioning accuracy with MicroPositioning Robots (MPRs) is required to successfully perform many complex tasks, such as micro-assembly, manipulation and characterization of biological tissues, and minimally invasive inspection and surgery. Despite the widespread use of high-resolution micro- and nanopositioning robots, there is very little knowledge about the real positioning accuracy that can be obtained and what the main influential factors are. Indeed, very few notable methods are available to measure multi-degree-of-freedom motions with adapted range, resolution, and dynamic capabilities.**

The main objective of the paper is to quantify the positioning accuracy of serial MPRs and to identify the main influential factors (a typical XYΘ serial robot is chosen as a case study). To reach this goal, a measuring system that combines vision and pseudo-periodic patterns with an extremely large range-to-resolution ratio is introduced as a new way to quantify the positioning accuracy of MPRs for in-plane motions. Then, an open loop control approach based on MPR calibration is chosen for several reasons: the use of different models to identify influential factors, the quantification of the positioning accuracy, and the necessity of the method when sensor integration is too complex. Experiments using five different calibration models were conducted to classify factors influencing the positioning accuracy of MPRs. The results show that positioning accuracy can be improved by more than 35 times from 96 μm with no imperfection compensation to 2.5 μm by compensating for geometric, position-dependent, and angle-dependent errors through the MPR calibration approach.

***Index Terms*—Micropositioning robots, microrobotic calibration, open loop, accuracy, serial robot.**

I. Introduction

Achieving highly accurate and reliable position control with MicroPositioning Robots (MPRs) is required to successfully perform many complex tasks, such as microassembly [1], [2], characterization of microscale components [3], biological micromanipulation [4], [5], specimen handling [6], microdispensing [7], and laser [8] or AFM scanning [9]. Considering many factors (e.g., success rate, speed, and contamination), these tasks usually rely on MPRs with automatic control, semi-automatic control, or teleoperation instead of manual operation [10]–[13]. Positioning accuracy is a key criterion of MPRs because it directly impacts the performance and capabilities. Similar to macrorobots [14]–[16], MPRs have high repeatability, but accuracy can become an issue when reaching any specific target positions or orientations rather than only taught positions. For instance, in the MOEMS field, the coupling of monomode fibers or the assembly of a micro-interferometer requires assembly with relative positioning accuracy better than 1 μm to enable sufficient product performance [17] [18]. Such accuracy can be achieved by using micro- and nanorobots, which enable motions to be generated with extremely high repeatability (often below tens of nanometers). Nevertheless, many factors directly result in low positioning accuracy at the microscale [19]. For instance:

- A 0.1° Perpendicularity error between the X and Y axes induces 20 μm of positioning error of the robot end-effector over a 20-millimeter motion
- A 150-μrad yaw deviation during a linear motion induces about 5 μm of positioning error in the robot end-effector.

Such sources of inaccuracies accumulate due to the widespread use of a coarse-fine positioning principle that combines several micropositioning stages (friction-based guidance stages that generally include mechanical motion transformation) and nanopositioning stages (guidance stages based on compliant and backlash-free structures moved by active-material-based actuators). The effects of imperfections increase substantially with the complexity of robotic structures. This problem becomes more complicated when the robotic structures in many microscale applications are required to have more than 10 Degrees-of-Freedom (DoF) [20], [21].

Several works investigated the improvement of positioning accuracy for MPRs and showed that an intrinsic positioning accuracy of several tens of micrometers can be obtained (without any external sensors) [20], [22], [23]. These works mainly relied on vision-based measurement, which offers multi-DoF measurements (in the plane for one camera) but suffers from a severe range-to-resolution ratio trade-off (which is often used to measure motion ranges of several millimeters with μm range resolution). They also used black-box or semi-black-box modelling, which enables consideration of many possible influential parameters at the same time but induces difficulties to understand what the most influential factors are and to quantify the influence of each factor. Several works also investigated the issue of tolerance analysis in fields such as machine tools and microrobotics. Pac and Popa used interval analysis to bound the error that accumulates at the end-effector of a serial manipulator (a $XY\Theta$ structure was chosen as a case study) [24]. This study highlights that MPRs may have very large error bounds because many uncertainties accumulate, and every uncertainty cannot be identified precisely enough at the microscale.

N. Tan, C. Clévy, G. J. Laurent and N. Chaillet are with the FEMTO-ST Institute, AS2M department, Univ. Bourgogne Franche-Comté, Univ. de Franche-Comté/CNRS/ENSMM, 24 rue Savary, F-25000 Besanon, France. P. Sandoz is with the Applied Mechanics departement, also within the FEMTO-ST Institute emails: {cclevy, glaurent, patrick.sandoz, nchaillet}@femto-st.fr.

These different studies show several key difficulties and complexities: (i) successfully performing meaningful multi-DoF measurements with enough range-to-resolution ratio, (ii) understanding what the factors that influence positioning accuracy are and quantifying their real effects, and (iii) quantifying the positioning accuracy that can really be achieved with MPRs. This paper intends to address these three key issues, to clarify the typical behavior of MPRs, and to quantify their actual potential in terms of positioning accuracy when factors influencing their accuracy are compensated.

First, an original measurement setup is used. It relies on a principle introduced by Sandoz for biological sample localization purposes [25]. It is based on a camera (which is usually already integrated in most applications with MPRs) that is mounted onto a microscope and looks at a pseudo-periodic pattern. A dedicated algorithm based on phase measurements and binary coding provides position measurement of the pattern with very high range-to-resolution ratio as well as simultaneous measurements of the three DoF of the plane. This principle has been used and adapted for robotic purposes in previous work [26]. The method appears very promising for microrobotics or microsystems because it typically provides high resolution (typically a thousandth of a pixel), possible infinite range, self-calibration, and 3 DoF (in-plane) measurement. A case study of an $XY\Theta$ MPR is investigated using this principle for several reasons: widespread use, widespread study, adequate measurement capabilities, and the presence of all kinds of imperfections that can be met at the microscale.

Several calibration models are used to integrate the compensation of different parameters that may influence the positioning accuracy of the MPR. Experiments using these different models and related robot calibration enable quantification of the positioning accuracy that can be achieved for each case. Finally, the results are compared and analyzed to understand the main parameters that influence the positioning accuracy of MPRs, as well as to quantify their influence and the final positioning accuracy that can be achieved.

The remainder of this paper is organized as follows. Section II provides the typology of imperfections that are considered throughout the paper based on a usual typology for macroscale robotics and known microscale specificities and behaviors. Section III presents the measuring system based on a pseudo-periodic pattern. Geometric models and calibration procedures are presented in Section IV, while parameter identification is discussed in Section V. Section VI presents the experimental setup and MPR positioning accuracy results. Influential geometric parameters are presented in Section VI. Finally, the paper is concluded in Section VII.

II. Typology of Geometric Imperfections of Microrobotic Structures

MPRs are widespread in microscale applications. They are based on stick slip piezoelectric actuation or DC motors and have some common features [10]. For example, MPRs usually rely on a friction-based mechanical guiding principle (in contrast to nanopositioning systems, which are based on compliant joint linkages). The MPR imperfections or unknown parameters can be classified into three types:

1) The assembly errors between stages
2) The position-dependent errors along the translation axis
3) The angle-dependent errors induced by the rotation axis

These three types of imperfections are geometric errors. Dynamic parameters are less significant for MPRs and are not considered in this work.

The first type of error is shown in Fig. 1a. We assume that a joint axis that is attached to a frame $\{O_k, \vec{x}_k, \vec{y}_k, \vec{z}_k\}$ links with an adjacent axis attached to a frame $\{O_{k+1}, \vec{x}_{k+1}, \vec{y}_{k+1}, \vec{z}_{k+1}\}$. Three parameters a_k, b_k, and c_k depict their relative positions along the $\vec{x}_k$, $\vec{y}_k$, and $\vec{z}_k$ axes. Another three parameters α_k, β_k and γ_k depict their relative orientations. These parameters are affected by the assembly process and are called assembly parameters.

The second type of error is local imperfections along a translation axis (e.g., the $\vec{x}_k$ axis in the case shown in Fig. 1b). Because the motions of micropositioning axes are not perfectly linear, the commanded positions are not equal to the positions actually reached, and there are coupling errors on one axis when the motion happens on another axis. For a given joint input q_k, there are three translation errors and three rotation errors along the axis. The real position along the axis is $q_k + a_k(q_k)$, which is accompanied by coupling errors $b_k(q_k)$ and $c_k(q_k)$ along $\vec{y}_k$ and $\vec{z}_k$, respectively. Meanwhile, there are three angular imperfections $\alpha_k(q_k)$, $\beta_k(q_k)$, and $\gamma_k(q_k)$ in the motion.

The counterparts of a rotation axis are shown in Fig. 1c. Depending on the rotating angle q_k, the rotation center changes in 3-dimensional space. This eccentricity is defined with three positions $a_k(q_k)$, $b_k(q_k)$, and $c_k(q_k)$. Rotation motion may also generate angular-dependent errors in three directions, which are $q_k + \alpha_k(q_k)$, $\beta_k(q_k)$, and $\gamma_k(q_k)$.

These imperfections have different influences on positioning accuracy. In the following case study, we construct different models that consider the imperfections to quantify their influence on positioning accuracy.

III. In-plane visual measurement using pseudo-periodic pattern

Most high-resolution imaged-based motion-detection algorithms rely on phase-like correlation methods. For example, such a method has been implemented by Moddemeijer [27], who reported a resolution of 13.3 nm. The main drawback of these correlation-like methods is the useful field of view. Such methods are feature-dependent, so the pattern has to remain inside the region of interest to be analyzed, which limits the range of measurement. To overcome this drawback, techniques based on pseudo-periodic patterns have been proposed [25], [28], [29].

One method [25] is based on an encryption of a binary code over a pseudo-periodic pattern (PPP). The position is obtained by combining fine and coarse measurements that are complementary. The fine measurement is performed after a 2D Fourier transformation to separate the different directions of modulation of the pattern. The phase of the periodic grid is then computed in both directions using two analysis functions.

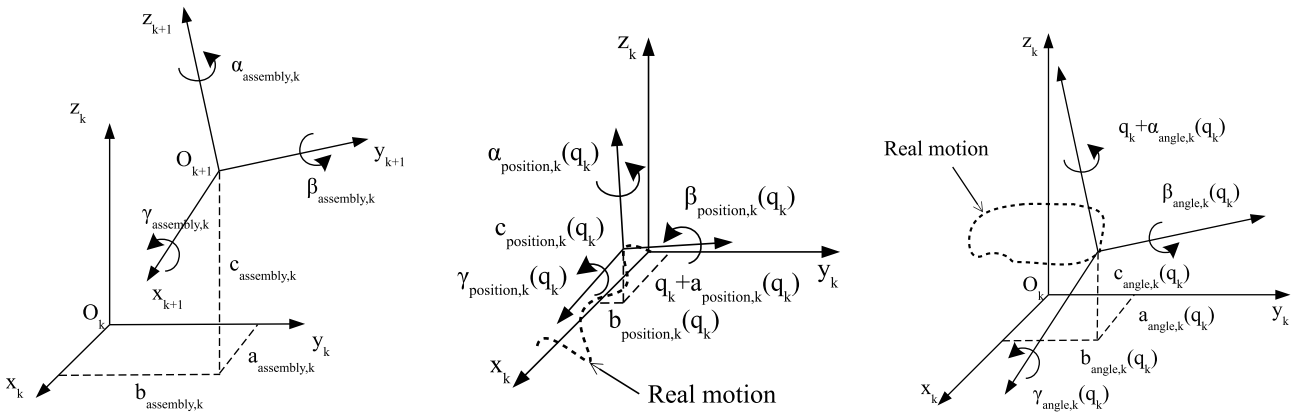

(a) Assembly errors between two stages (b) Position-dependent errors along a prismatic joint (c) Angle-dependent errors about a revolute joint

Fig. 1. Typology of geometric imperfections of microrobotic structures ($\{O_k, \vec{x}_k, \vec{y}_k, \vec{z}_k\}$ is the frame attached to the base part joint k and $\{O_{k+1}, \vec{x}_{k+1}, \vec{y}_{k+1}, \vec{z}_{k+1}\}$ the frame of mobile part of a joint or to the next stage for the case a).

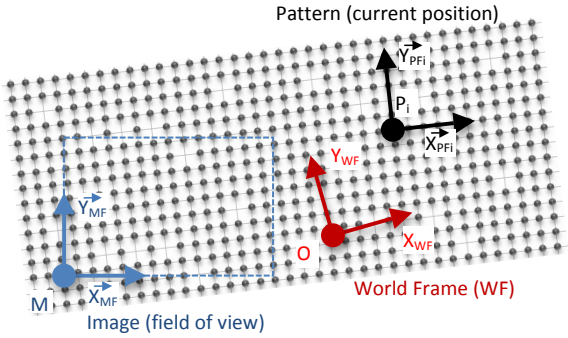

Fig. 2. Frames definition for the measurement: image frame which is also the frame in which the measurement are provided (MF), the pattern frame (PF) and the world frame (WF) which is the initial pattern frame location.

Given the phases (in rad) and the period of the pattern (in meters), it is straightforward to calculate the relative position of the pattern in the image reference frame. This process gives the position with a typical subpixel resolution of 10^{-3} pixels but also with an indeterminacy equal to the wavelength of the pattern.

The coding allows for absolute but coarse coordinate transformations of the image reference frame into actual positions on the observed part of the pattern. This codification is based on linear feedback register sequences (LFRS). Pose retrieval involves complementary image processing to identify the location of the missing points and thus to return the line and column orders necessary to obtain the fine position provided by phase computations.

The measuring range is limited by the size of the pattern, which is 9.5 mm for the x-axis and 4.2 mm for the y-axis in the present case. The repeatability of the visual measurement has been experimentally evaluated and is better than 10 nm [30]. More details about the algorithm and the fabrication of the pattern can be found in another study [31].

We propose using this technique to characterize the in-plane motion of MPRs. There is great interest in using the method for MPR calibration. The method is a non-contact measurement and thus does not affect the motion of the robot. Also, there is no need to calibrate the imaging system, which is a delicate task at this scale. Indeed, as the period of the pattern is precisely known (4 μm in the present case), the measurement is intrinsically self-calibrated. Finally, the most interesting point is that the method is able to measure 3-DoF in-plane displacements simultaneously. This allows the position-dependent errors of the stages to be measured along X, Y, and Θ with accuracy that has only been achieved before in one direction using interferometry.

The pattern is fixed on a substrate located on the rotation stage Θ. A part of this pattern is seen in the field of view of the vision system (Fig. 2). In this paper, M is named as the origin of the image frame $\{M, x_{MF}, y_{MF}\}$. Based on these images and their processing, the positions (x_{mi}, y_{mi}) and orientation (Θ_{mi}, clockwise) of the pattern are measured in the image frame. Subscript m refers to data issued from experimental measurement, while subscript i refers to the i^{th} measurement achieved. The pattern frame PF $\{P_i, x_{PF_i}, y_{PF_i}, z_{PF_i}\}$ is thus the current location of the pattern. PF is considered as the tool frame, which is moving with different configurations or poses of the MPR. The origin P of the pattern is considered as the tool tip of the end-effector and is the point of interest to be controlled. Finally, the world frame WF $\{O_{WF}, x_{WF}, y_{WF}, z_{WF}\}$ is defined as the initial location of the pattern, i.e. $WF = PF_{(when\ i=0)}$. The position of O_{WF} is then defined by x_{m0}, y_{m0}, and Θ_{m0} in the MF frame. Based on x_{m0}, y_{m0}, Θ_{m0}, x_{mi}, y_{mi}, and Θ_{mi}, the coordinates of P_i in WF can be defined by x_{Pmi} and y_{Pmi} as follows:

$$\begin{bmatrix} x_{Pmi} \\ y_{Pmi} \end{bmatrix} = \begin{bmatrix} \cos(\Theta_i) & \sin(\Theta_i) \\ -\sin(\Theta_i) & \cos(\Theta_i) \end{bmatrix} \cdot \begin{bmatrix} x_{mi} - x_{m0} \\ y_{mi} - y_{m0} \end{bmatrix} \quad (1)$$

IV. Calibration Models and Procedures

MPRs generally consist of an assembly of translation and rotation axes that suffer from the imperfections mentioned in

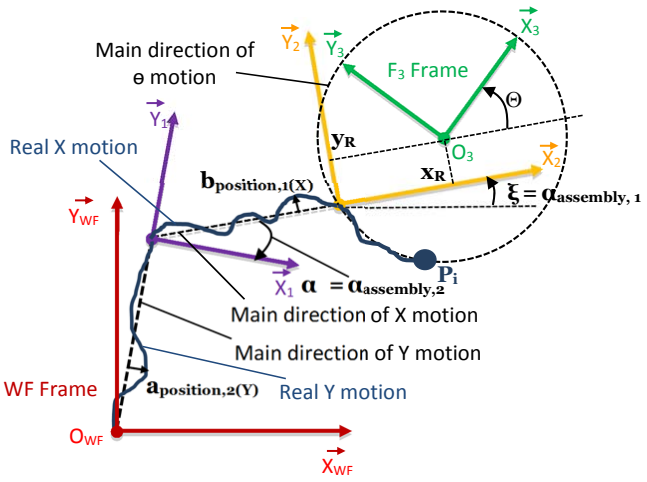

Fig. 3. Frames definition of the kinematics including parameters to be identified.

Fig. 1. Without loss of generality, an XYΘ MPR is chosen as a typical case study. Based on commonly used devices for microscale applications, this XYΘ structure faces all imperfection types mentioned.

A. Definition of frames

The stages are assembled in series of Y, X and Θ where the Y stage is on the bottom and the Θ stage is on the top. Fig. 3 displays the frames used to define the kinematics of the XYΘ stage used. Frames F_1 $\{O_1, x_1, y_1, z_1\}$ and F_2 $\{O_2, x_2, y_2, z_2\}$ are assigned to the mobile parts of the Y and X stages, respectively. The Y motion is along y_1, and the X motion is along x_2. The frame F_3 $\{O_3, x_3, y_3, z_3\}$ is attached to the mobile part of the Θ stage. The Θ motion rotates clockwise about z_3. In the initial state, all the frames are superimposed on the world frame WF.

B. Forward and inverse kinematics

Because the external reference system can only measure in-plane motions, we do not consider the out-of-plane imperfections (c_k, β_k and γ_k). In addition, some of the imperfections cannot be identified independently from the others. So, we selected a combination of imperfections that are directly identifiable and that are sufficient to calibrate the complete kinematics.

The assembly errors between the three axes are represented by four parameters:

- ξ is the alignment angle between x_{WF} and x_2 which is 180° in the ideal case; and includes the assembly error between the stage X (F_2 Frame) and the rotation stage (F_3 Frame) on which is fixed the pattern (i.e. $\xi = \alpha_{assembly,1}$)
- α is the perpendicularity error between the X stage and Y stage, which is also the angle between x_1 and x_2 (i.e. $\alpha = \alpha_{assembly,2}$), $\alpha = 0$ in the ideal case
- (x_R, y_R) are the coordinates of the rotation center O_3 with respect to F_3 (F_3 is superimposed on the world frame at the beginning).

The position- and angle-dependent errors are also represented by four parameters:

- ex and ey are the combinations of position-dependent errors along stages X and Y;
  i.e. $ex = a_{position,1}(X) - a_{position,2}(Y)\sin(\alpha)$
  and $ey = b_{position,1}(X) + b_{position,2}(Y)\cos(\alpha)$;
- h_{ax} and h_{ay} are the angle-dependent errors for the rotation stage

Given joint coordinates $q_1 = Y$, $q_2 = X$, and $q_3 = \Theta$ and parameters $\phi = \{x_R, y_R, \xi, \alpha\}$, and considering ex, ey, h_{ax}, and h_{ay}, the coordinates of end point P_i $\{x_P, y_P\}$ in the world frame could be calculated by:

$$\begin{bmatrix} x_P \\ y_P \end{bmatrix} = \begin{bmatrix} (X-ex)\cos(\xi) - (Y-ey)\sin(\xi+\alpha) \\ +x_R + h_{ax}(\Theta) - x_R\cos(\Theta) - y_R\sin(\Theta) \\ (X-ex)\sin(\xi) + (Y-ey)\cos(\xi+\alpha) \\ +y_R + h_{ay}(\Theta) + x_R\sin(\Theta) - y_R\cos(\Theta) \end{bmatrix}, \quad (2)$$

which is the forward kinematics of the MPR. ex and ey are the corresponding position-dependent errors of coordinate (X,Y). $h_{ax}(\Theta)$ and $h_{ay}(\Theta)$ are angle-dependent errors when the rotation angle equals Θ. Then, the inverse kinematics can be obtained accordingly:

$$\begin{bmatrix} X \\ Y \end{bmatrix} = \begin{bmatrix} \frac{1}{\cos(\alpha)}\big(x_P\cos(\xi+\alpha) + y_P\sin(\xi+\alpha) \\ -x_R\cos(\xi+\alpha) - y_R\sin(\xi+\alpha) \\ +x_R\cos(\Theta+\xi+\alpha) + y_R\sin(\Theta+\xi+\alpha)\big) \\ +g_{ax} + ex \\ \frac{1}{\cos(\alpha)}\big(-x_P\sin(\xi) + y_P\cos(\xi) \\ +x_R\sin(\xi) - y_R\cos(\xi) - x_R\sin(\Theta+\xi) \\ +y_R\cos(\Theta+\xi)\big) + g_{ay} + ey \end{bmatrix}, \quad (3)$$

where $g_{ax}(\Theta)$ and $g_{ay}(\Theta)$ are the inverse increments of $h_{ax}(\Theta)$ and $h_{ay}(\Theta)$ provided to the joint input, respectively.

We chose lookup tables to construct the position- and angle-dependent error functions. Linear interpolation is used when a value is not inside the lookup table.

C. Calibration models and procedures

We propose five models to investigate the influence of every imperfection on the positioning accuracy of the whole robot.

First, for a MPR with a rotation axis, the location of the rotation center is the desired knowledge for modeling and control. So, the first model (Model I) considers the basic parameters identified as x_R and y_R. The nominal values $\xi = 180°$ and $\alpha = 0°$ are used as alignment and assembly parameters. The position- and angle-dependent errors are zero. This model considers the minimum requirements of modeling while ignoring other errors and could also be called the basic geometric model. In addition to the basic parameters x_R and y_R, Model II also addresses the inaccuracy induced by alignment parameter ξ and assembly error α.

As an enhanced version of Model II, Model III compensates errors along X and Y considering microscale specificities, namely, the position-dependent errors ex and ey.

To quantify ex and ey, a preliminary experiment is performed, and values of ex and ey are obtained as a set of discrete points along the X and Y axes. One-dimensional lookup tables are built for each errors along each axis. It is then

easy to interpret errors stored in tables but also to reuse them even if the assembly of stages is different. Linear interpolation is used to calculate the corresponding ex and ey at the points not measured.

Instead of position-dependent errors, Model IV (another enhancement of Model II) directly compensates angle-dependent errors induced by Θ motion.

Finally, the most advanced model (Model V) takes into account all four kinds of imperfections.

In summary, different models address different sets of the mentioned imperfections. Their corresponding relations are summarized in Table I. The model complexity increases from Model I to Model V.

Model I and Model II follow the conventional calibration procedure (1. Modeling, 2. Data acquisition, 3. Identification, 4. Implementation, 5. Validation). A pre-calibration step has been introduced before parameter identification for Models III, IV, and V. For these models, the position-dependent errors are measured for each axis and added to the joint input during the identification and implementation phases using interpolated functions.

V. Parameter identification

Parameter identification is performed in four steps. First, a cost function is built to include calculated poses and measured poses. Second, the identifiability of the parameters is examined. Third, observability analysis is performed to estimate the optimal number of poses. The last step is to identify the parameters through minimizing the cost function. The second and third steps are investigated through simulation. The last step is performed with experimental data and discussed in section VI, while the first three steps are discussed in detail in the following.

A. Cost functions

Parameters are identified through minimizing the error between measured position (given in the WF) $P_{mi}\{x_{Pmi}, y_{Pmi}\}$ and calculated position P_{ci}. P_{ci} is calculated through forward kinematics using Eq. (2), that is, $P_{ci} = P_i$. The i^{th} element of the cost function is defined as:

$$e_i = \varepsilon_{x_i}^2 + \varepsilon_{y_i}^2$$

where:

$$\begin{cases} \varepsilon_{x_i} = x_{Pi} - x_{Pmi} \\ \varepsilon_{y_i} = y_{Pi} - y_{Pmi} \end{cases} \tag{4}$$

Initial pose coordinates x_{m0} and y_{m0} can be eliminated by subtracting two poses:

$$\begin{cases} \varepsilon_{x_{i,j}} = \varepsilon_{x_i} - \varepsilon_{x_j} \\ \varepsilon_{y_{i,j}} = \varepsilon_{y_i} - \varepsilon_{y_j} \end{cases} \tag{5}$$

x_{Pi} and y_{Pi} can be obtained by forward kinematics (2). The following cost function E can be defined with different pose combinations for n poses:

$$E = \varepsilon^T \varepsilon \tag{6}$$

where:

$$\varepsilon = \begin{bmatrix} \varepsilon_{x_{1,2}} \\ \varepsilon_{y_{1,2}} \\ \varepsilon_{x_{2,3}} \\ \varepsilon_{y_{2,3}} \\ \vdots \\ \varepsilon_{x_{n-1,n}} \\ \varepsilon_{y_{n-1,n}} \end{bmatrix}, \text{with } 2(n-1) \text{ elements.}$$

Parameter identification turns into an optimization problem minimizing E.

B. Identifiability analysis

Identifiability analysis evaluates how much the parameters are identifiable [32]. The determination of the identifiable parameters must be done before the identification process. Equation (2) can be written in a general form $f(q, \phi) = P$ (where q is the vector of joint coordinates, ϕ is the vector of kinematic parameters, and P is the vector of tool coordinates). The equation can be linearized as:

$$\Delta P = \frac{\partial f}{\partial \phi} \Delta \phi. \tag{7}$$

For the i^{th}, j^{th} pair poses, the Jacobian of $\varepsilon_{i,j}$ is:

$$J_{i,j} = \begin{bmatrix} \frac{\partial \varepsilon_{x_{i,j}}}{\partial x_R} & \frac{\partial \varepsilon_{x_{i,j}}}{\partial y_R} & \frac{\partial \varepsilon_{x_{i,j}}}{\partial \xi} & \frac{\partial \varepsilon_{x_{i,j}}}{\partial \alpha} \\ \frac{\partial \varepsilon_{y_{i,j}}}{\partial x_R} & \frac{\partial \varepsilon_{y_{i,j}}}{\partial y_R} & \frac{\partial \varepsilon_{y_{i,j}}}{\partial \xi} & \frac{\partial \varepsilon_{y_{i,j}}}{\partial \alpha} \end{bmatrix}. \tag{8}$$

Through QR decomposition [33]:

$$QR = J.$$

An upper triangular matrix R is obtained where the elements on the diagonal correspond to the kinematic parameters. The non-identifiable parameters are those equal to zero. In this case, all elements on the diagonal are not equal to zero, which means all parameters are identifiable. QR decomposition of (8) can be done through simulation. One example of the simulation results is:

$$R = \begin{bmatrix} 2.0077 & -1.7347\text{e-}18 & 0.5169 & 8.2052\text{e-}18 \\ & 2.0077 & 0.0158 & 8.3210\text{e-}17 \\ & \mathbf{0} & -464.5673 & -72.7559 \\ & & & 168.8389 \end{bmatrix}.$$

The matrix demonstrates that all four geometric parameters are identifiable for two cost functions using randomly generated poses.

C. Observability analysis

To identify unknown parameters, a set of poses is chosen and measurements are performed at these poses. In the expertise of robotic calibration, observability index measures the quality of the poses chosen. The observability index is based on singular values by Singular Value Decomposition (SVD) [34]. For a problem with m parameters, n poses, and 2-dimensional measurements, applying SVD to the Jacobian yields:

$$J = U \Sigma V^T \tag{9}$$

TABLE I
TABLE OF ERRORS AND PARAMETERS CONSIDERED BY THE FIVE CALIBRATION MODELS (POSITION-DEPENDENT AND ANGLE-DEPENDENT ERRORS ARE COMPENSATED USING ONE-DIMENSIONAL LOOKUP TABLES).

Calibration Model	Rotation center		Assembly parameters		Position-dependent errors		Angle-dependent errors		Model complexity
	x_R	y_R	ξ	α	ex	ey	h_{ax}	h_{ay}	
Model I: Basic geometric	$\star$	$\star$	180	0	0	0	0	0	$\star$
Model II: Geometric	$\star$	$\star$	$\star$	$\star$	0	0	0	0	$\star\star$
Model III: Geometric + position-dependent	$\star$	$\star$	$\star$	$\star$	$\star$	$\star$	0	0	$\star\star\star$
Model IV: Geometric + angle-dependent	$\star$	$\star$	$\star$	$\star$	0	0	$\star$	$\star$	$\star\star\star$
Model V: Geometric + position-dependent +angle-dependent	$\star$	$\star$	$\star$	$\star$	$\star$	$\star$	$\star$	$\star$	$\star\star\star\star\star$

where U is a $2n \times 2n$ orthogonal matrix, V is an $m \times m$ orthogonal matrix, and Σ is the $2n \times m$ matrix of singular values:

$$\Sigma = \begin{bmatrix} S \\ 0_{2n-m,m} \end{bmatrix}, \tag{10}$$

where:

$$S = \begin{bmatrix} \sigma_1 & 0 & 0 & \cdots & 0 \\ 0 & \sigma_2 & 0 & \cdots & 0 \\ \vdots & \vdots & \vdots & \vdots & \vdots \\ 0 & 0 & 0 & \cdots & \sigma_m \end{bmatrix} \tag{11}$$

is a $m \times m$ matrix of ordered singular values, with $\sigma_1 \geq \sigma_2 \geq \cdots \geq \sigma_m \geq 0$. Four observability indices have been previously proposed [34]–[36], which are denoted by O_1, O_2, O_3 and O_4.

Borm and Menq [37] proposed an observability index termed O_1 that maximizes the product of all of the singular values:

$$O_1 = \frac{\sqrt[m]{\sigma_1 \sigma_2 \cdots \sigma_m}}{m}. \tag{12}$$

Index O_2 [38] is the ratio of the minimum singular value to the maximum singular value:

$$O_2 = \frac{\sigma_m}{\sigma_1}. \tag{13}$$

Index O_3 [39] is the minimum singular value:

$$O_3 = \sigma_m. \tag{14}$$

Index O_4 [39] is the product of O_2 and O_3 which is termed the noise amplification index:

$$O_4 = \frac{\sigma_m^2}{\sigma_1}. \tag{15}$$

Based on maximization of these indices, the optimal number of poses and optimal poses can be selected. Fig. 4 shows the simulation results of observability with increasing number of random poses for the cost function E. Among these indices, O_3 only takes into account the minimum singular value instead of both minimum and maximum singular values. Index O_1 was found to be worse than the others [39]. Hence, we mainly consider indices O_2 and O_4. However, there is no obvious change in index O_2 after about 400 poses, indicating that this number is the minimum. Meanwhile, the slope of the index O_4 curve becomes smaller and smaller, which means taking more poses becomes less and less important. Moreover, index O_4 is an indicator of the amplification of sensor noise. To balance the best number and the elimination of sensor noise, a trade-off between O_2 and O_4 is made such that 1200 pairs of measurements will be taken (each pair includes x_m and y_m).

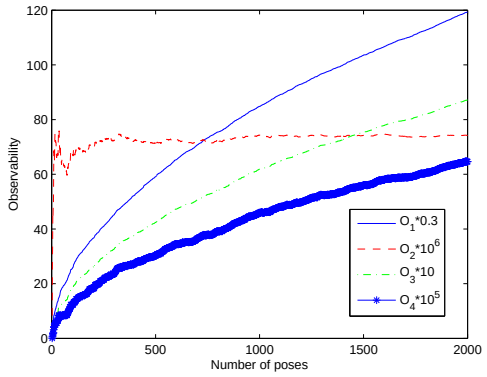

Fig. 4. Observability of cost function E with 3 to 2000 poses.

VI. EXPERIMENTAL IDENTIFICATION AND VALIDATION

This section aims at identifying factors that influence the positioning accuracy through quantifying the positioning accuracy with and without compensation of these factors. This quantification is done through experimentations based on the five models previously defined.

A. Experimental setup

Pictures of the whole experimental setup and the end-platform (supporting the substrate) are shown in Fig. 5. The MPR is mounted on an anti-vibration table. It consists of two translation stages (X and Y) and a rotation stage (Θ) in a 3-DoF serial robotic structure. The two translation stages are PI M-111.1DG stages equipped with a Mercury TM C-863 controller. This kind of stage is representative of many

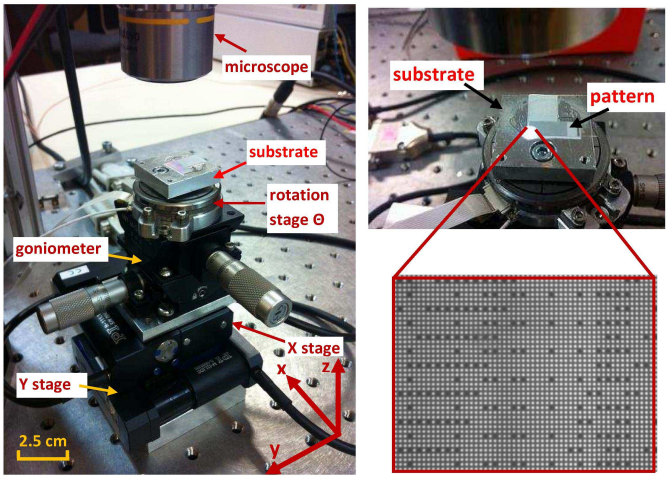

Fig. 5. Large and close view of the XYΘ MPR used as experimental case study. The microscope provides a top view of the pattern which is attached on the substrate.

TABLE II
SPECIFICATION OF XY TRANSLATION STAGES IN DATASHEET

Stage	PI M-111.1DG
Travel range	15 mm
Resolution	50 nm
Unidirectional repeatability	100 nm
Pitch angle deviation	$\pm 150\ \mu rad$
Yaw angle deviation	$\pm 150\ \mu rad$
Backlash	$2\ \mu m$
Thread pitch	0.4 mm
Driving mechanism	Leadscrew

micropositioning stages commonly used in micromanipulation and work with mobile parts that are guided based on friction principles. The rotary stage is a SmarAct SR-3610-S controlled by an MCS-3D unit. All the micropositioning stages X, Y, and Θ are equipped with internal sensors and are already controlled with a closed-loop controller in the actuator layers (since the integration of sensors in MPRs is highly challenging, pure direct measurement remains quite rare at this scale). The datasheet specifications of the translation stages X and Y and rotation stage Θ are given in Tables II and III, respectively.

The external measuring reference system for calibration consists of a video camera (AVT STINGRAY F-125C 1024×768 mono), a microscope tube (Optem zoom 70XL), and an objective with 10× magnification. An upper goniometer (M-GON40-U) and lower goniometer (M-GON40-L) are used for adjusting the parallelism between the pattern and the camera.

Temperature was measured during experiments but no observable dependency was noticed.

B. Data acquisition and parameter identification

To identify the kinematic parameters in (2), the first step is to acquire measuring information of the end-point. During the data acquisition phase, the MPR is commanded to reach a set of configurations by changing the translations and rotation joint coordinates. Meanwhile, the vision system captures all

TABLE III
SPECIFICATION OF Θ ROTATION STAGE IN DATASHEET

Stage	SmarAct SR-3610-S
Range	360 °
Stepwidth	$0.3\ m°$ to $3\ m°$
Scanning range	$\simeq 4.3\ m°$
Resolution	$< 1.1\ \mu°$

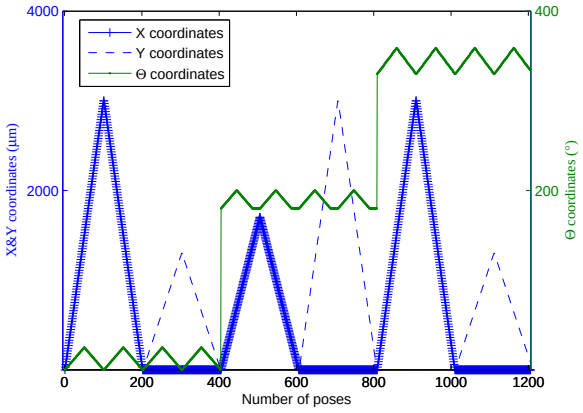

Fig. 6. Joint coordinates of XYΘ stages in data acquisition.

the images of the poses and retrieves the measuring information. The defined trajectories of the joint axes are shown in Fig. 6. This process takes about 1.3 hours. The number of measurements is chosen based on the presented observability analysis. A total of 1200 pairs of measurements are obtained in the data acquisition phase.

Geometric parameters are identified by solving a nonlinear least-squares problem (using Matlab® function $lsqnonlin$). After identification, the parameters for five models are obtained as shown in Table IV. The modification of the joint coordinates of the X and Y axes considering position-dependent errors induces small differences in the identified parameters between Model II and Model III. Models II and IV use the same values for these four parameters. The four parameters of Models III and V are the same. The identified results have to be validated by implementing them in the inverse kinematics of the MPR.

C. Models comparison

To compare the positioning accuracy of the MPR using different calibration models, 9 target points are chosen in

TABLE IV
TABLE OF PARAMETERS FOR FIVE MODELS

Identified parameters	$x_R(\mu m)$	$y_R(\mu m)$	$\xi(°)$	$\alpha(°)$
Model I	9572.902	7795.830	180	0
Model II	9572.902	7795.830	177.689	-0.132
Model III	9572.904	7795.858	177.685	-0.107
Model IV	9572.902	7795.830	177.689	-0.132
Model V	9572.904	7795.858	177.685	-0.107

TABLE V
TABLE OF 9 TARGET POINTS AND ROTATION ANGLES FOR VALIDATION

Targets P_T	$x_T(\mu m)$	$y_T(\mu m)$	$\Theta_T(^\circ)$
P_1	-1200	-200	1
P_2	-1600	-200	2
P_3	-2000	-200	3
P_4	-2000	-300	4
P_5	-1600	-300	5
P_6	-1200	-300	4
P_7	-1200	-400	3
P_8	-1600	-400	2
P_9	-2000	-400	1

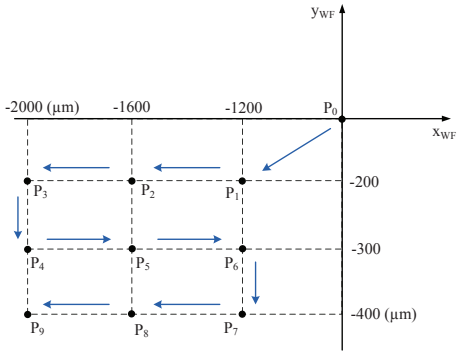

Fig. 7. Moving sequence of target points (P_T) in validation.

the world frame that cover the working range of the robot (Table V). The trajectory of validation follows P_0, P_1, ..., P_9, which is shown in Fig. 7. As shown in Fig. 8, the signal is processed with the following procedure: 1) The target $P_T\{x_T, y_T, \Theta_T\}$ is fed into the inverse kinematics, and the corresponding joint input P_c of the MPR can be calculated; 2) the MPR moves under the command P_c; 3) the measuring system saves the images and retrieves the measurement information D_{PF} in the pattern frame; and 4) the measurements are transformed into the value P_m with respect to the world frame.

The results of positioning accuracy of the MPR are shown in Fig. 9 and Table VI, where the larger the accuracy value is, the worse the accuracy of the robot is. Several experiments show that the repeatability is always smaller than 0.8 μm and is quite constant, regardless of the pose and the time.

The positioning accuracy using Model I is approximately 100 μm. The positioning error becomes larger at the points farther from the origin of the world frame, which means that the accuracy is highly influenced by the amplitudes of X and Y motions. This is due to the alignment parameter ξ and assembly error α not being considered in the model. The greater the distance between the targets and the origin P_0,

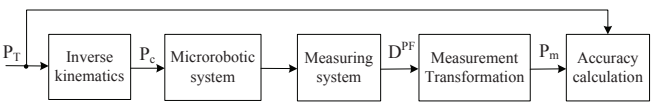

Fig. 8. Block diagram of validation procedure.

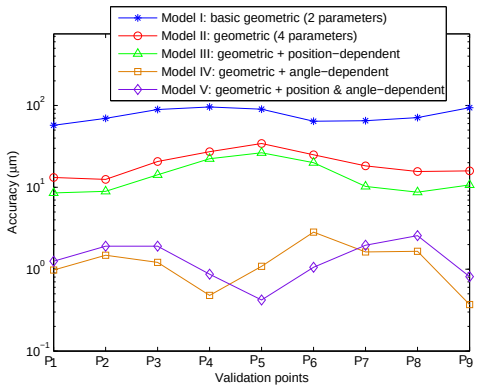

Fig. 9. Experimental results of positioning errors using five models on a logarithmic scale.

TABLE VI
TABLE OF ACCURACY OF DIFFERENT CALIBRATION MODELS

Accuracy	X axis (μm)	Y axis (μm)	XY plane (μm)
Model I	49.130	91.108	95.980
Model II	6.433	34.330	34.338
Model III	2.810	26.460	26.461
Model IV	0.940	2.677	2.838
Model V	1.651	2.122	2.568

the larger the induced errors by the two angles are.

The compensation of the errors of ξ and α greatly improves the accuracy, which reaches 35 μm. The accuracy curve achieved by Model II demonstrates no dependency on the distances between the targets and the origin, but there is a dependency on the rotation angles.

Compensation of the position-dependent errors along the X and Y axes can reduce inaccuracy further by nearly 10 μm with Model III. Similar to Model II, the accuracy curve of Model III also displays a dependency on the rotation angle. The accuracy increases with the rotation angles.

To quantify the angle-dependent errors $h_{ax}(\Theta)$ and $h_{ay}(\Theta)$ in Models II and III, an additional experiment is required to evaluate the residual errors. In the experiment, Models II and III are implemented to control the MPR while moving and following the target trajectory in Fig. 10. Every target position corresponds to 5 rotation angles. The positioning errors $h_{ax}(\Theta)$ and $h_{ay}(\Theta)$ at these poses form a lookup table, through which $g_{ax}(\Theta)$ and $g_{ay}(\Theta)$ are calculated using inverse kinematics and added to the joint coordinate inputs. When implementing Models IV and V, positioning accuracies of 2.8 and 2.5 μm are achieved. The accuracies achieved by Models IV and V are quite close because quantified angle-dependent

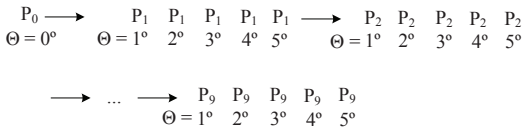

Fig. 10. Moving sequence of target points (P_T) in measuring angle-dependent errors $h_{ax}(\Theta)$ and $h_{ay}(\Theta)$.

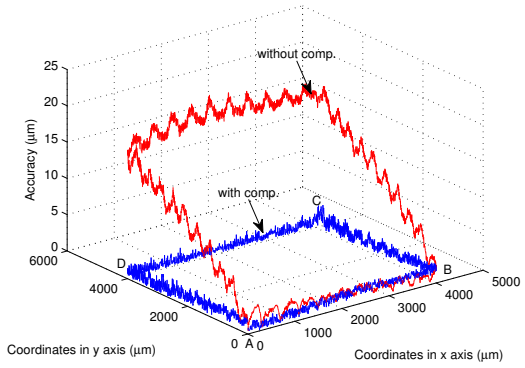

Fig. 11. Accuracy of tracking square with and without compensation (model III).

errors include a part of the position-dependent errors.

In summary, different imperfections have different ways of influencing accuracy and to different degrees. The model selection is a trade-off between model complexity and accuracy achieved. Model I is for the most basic application. It requires little imperfection compensation except for the position of the rotation center.

The most influential parameters are ξ and α. The positioning accuracy-to-cost ratio of Model II is high because these two parameters are easy to identify, and by compensating them, the accuracy improves by about 60% with Model II. Angle-dependent errors are also very significant. A 5° rotation induces nearly 20 μm of inaccuracy. To achieve the best positioning accuracy, Models IV and V should be chosen, and of course, more efforts must be made on measurement and calibration.

Position-dependent errors are less important than the other two kinds of imperfections, which generate inaccuracy of about 5 to 8 μm. However, Models II and III are less complex than Models IV and V. So, if only a medium level of accuracy is required, Models II and III are sufficient.

D. Full trajectory example

Model III was used to demonstrate the error compensation on a square trajectory without rotation. The trajectory is a 4000 $\times$ 4000 μm square spanning from coordinates 10 μm to 4010 μm. The square is divided into 4 segments: AB, BC, CD, and DA. The tracking performances with and without compensation are shown in Fig. 11.

The inaccuracy reaches about 22 μm without compensation, which is mainly due to the perpendicularity error (BC and DA segments) and to position-dependent errors (AB and CD segments). It can be seen that without compensation errors vary cyclically. Such behavior is reasonably due to systematic turn-to-turn nature inherent in the leadscrew. Indeed, the period of the error is equal to the thread pitch of the stage (400 μm).

After compensation, inaccuracy is reduced to approximate 4 μm.

VII. CONCLUSIONS

In microrobotics, positioning accuracy is a very important issue that is tightly correlated with system performance. However, there are many sources of inaccuracy in such systems. We investigated the influences of the main sources and quantified the positioning accuracy once the imperfections were compensated through calibration.

A 3-DoF serial-type MPR was chosen as a case study because of its popularity in microscale applications and because of the capabilities of the measuring system. The setup consists of a regular vision system observing a pseudo-periodic encoded pattern to measure the motion behavior of the XY micropositioning stages. This method is particularly suitable for microscale motion characterization thanks to its high range-to-resolution ratio and avoidance of camera calibration.

Five inaccuracy models was proposed to depict and control the XYΘ MPR. The five models took into account different sources of inaccuracy at the microscale, and different levels of accuracy were achieved. In many applications involving rotation stages, knowledge of the coordinates of the rotation center (x_R,y_R) are required. Model I is a basic model that meets this requirement. The most influential parameters ξ and α identified in Model II are mounting errors due to manual assembly. Models III, IV, and V are advanced models that compensate position- or/and angle-dependent errors.

Experimental validations of five models demonstrated substantial improvements of quasi-static positioning accuracy in the experimental results by a factor of 40 (from 96 μm to 2.5 μm). The number of measuring poses was determined based on observability analysis. In the case study, for required accuracy less than 100 μm, the alignment and perpendicularity errors could be neglected according to the results of Model I, and nominal values (zeros) were sufficient. For required accuracy smaller than 40 μm, these two errors must be compensated. A further reduction of about 10 μm can be achieved by Model III by compensating position-dependent errors along the X and Y axes. The best accuracies achieved by Models IV and V were below 5 μm with position- and angle-dependent error compensation. Nevertheless, position-dependent error compensation has no significant positive impact when angle-dependent errors are also compensated. In conclusion, the most significant sources of inaccuracy in order of descending influence are: the rotation center, alignment and assembly errors, angle-dependent errors, and position-dependent errors.

These results have been established for in-plane motions. The extension of the PPP algorithm to out-of-plane motions is not straightforward and requires further works. Improvements of the method could also concern the reduction of the amount of data required to compensate position and angle-dependent errors by using more advanced interpolation schemes.

VIII. ACKNOWLEDGMENTS

This work was funded by the Franche-Comte region, OSEO and partially supported by the Labex ACTION project (contract "ANR-11-LABX-0001-01") and by the French RENATECH network and its FEMTO-ST technological facility. We

would like to acknowledge D. Guibert for his technical support.

REFERENCES

[1] K. Rabenorosoa, C. Clévy, and P. Lutz, "Active force control for robotic micro-assembly: application to guiding tasks," in *IEEE International Conference on Robotics and Automation*, Anchorage, AK, USA, 2010, pp. 2137–2142.

[2] B. Tamadazte, S. Dembélé, and N. L. Fort-Piat, "Cad model-based tracking and 3d visual-based control for mems microassembly," *International Journal of Robotics Research*, vol. 29, no. 11, pp. 1416–1434, 2010.

[3] J. O. Abrahamians, B. Sauvet, J. P. Maris, R. Braive, and S. Régnier, "Nanorobotic system for in situ stiffness measurements on membranes," *IEEE Transactions on Robotics*, vol. 30, pp. 119–124, 2013.

[4] S. Hu and D. Sun, "Automatic transportation of biological cells with a robot-tweezer manipulation system," *International Journal of Robotics Research*, vol. 30, no. 14, pp. 1681–1694, 2011.

[5] R. Yang, B. Song, Z. Sun, K. W. C. Lai, C. K. M. Fung, K. C. Patterson, K. Seiffert-Sinha, A. A. Sinha, and N. Xi, "Cellular level robotic surgery: Nanodissection of intermediate filaments in live keratinocytes," *Nanomedicine: Nanotechnology, Biology and Medicine*, vol. 11, no. 1, pp. 137–145, 2015.

[6] P. Saketi, M. V. Essen, M. Mikczinski, S. Heinemann, S. Fatikow, and P. Kallio, "A flexible microrobotic platform for handling microscale specimens of fibrous materials for microscopic studies," *Journal of Microscopy*, vol. 248, no. 2, pp. 163–171, 2012.

[7] E. Griffith and S. Akella, "Coordinating multiple droplets in planar array digital microfluidic systems," *International Journal of Robotics Research*, vol. 24, no. 11, pp. 933–949, 2005.

[8] A. Espinosa, X. Zhang, K. Rabenorosoa, C. Clévy, S. R. Samuelson, B. Komati, H. Xie, and P. Lutz, "Piston motion performance analysis of a 3dof electrothermal mems scanner for medical applications," *nternational Journal of Optomechatronics*, vol. 8, no. 3, pp. 179–194, 2014.

[9] A. Requicha, D. Arbuckle, B. Mokaberi, and J. Yun, "Algorithms and software for nanomanipulation with atomic force microscopes," *International Journal of Robotics Research*, vol. 28, no. 4, pp. 512–522, 2009.

[10] N. Chaillet and S. Régnier, *Microrobotics for Micromanipulation*. Wiley-ISTE, 2010.

[11] K. Rabenorosoa, C. Clévy, Q. Chen, and P. Lutz, "Study of forces during micro-assembly tasks using two-sensing-fingers gripper," *IEEE/ASME Transactions on Mechatronics*, vol. 17, no. 5, pp. 811–821, 2012.

[12] Z. Ni, A. Bolopion, J. Agnus, R. Benosman, and S. Régnier, "Asynchronous event-based visual shape tracking for stable haptic feedback in microrobotics." *IEEE Transactions on Robotics*, vol. 2, pp. 1081 – 1089, 2012.

[13] J. Liu, Z. Gong, K. Tang, Z. Lu, C. Ru, J. Luo, S. Xie, and Y. Sun, "Locating end-effector tips in robotic micromanipulation," *IEEE Transactions on Robotics*, vol. 30, no. 1, pp. 125–130, 2014.

[14] Z. Roth, B. Mooring, and B. Ravani, "An overview of robot calibration," *IEEE Journal of Robotics and Automation*, vol. 3, no. 5, pp. 377–385, 1987.

[15] B. W. Mooring, Z. S. Roth, and R. M. Driels, *Fundamentals of manipulator calibration*. Wiley-Interscience, 1991.

[16] H. W. Stone, A. C. Sanderson, and C. P. Neuman, "Arm signature identification," in *IEEE Conference of Robotics and Automation*, 1986.

[17] D. Popa, R. Murthy, and A. Das, "M3-deterministic, multiscale, multirobot platform for microsystems packaging: Design and quasi-static precision evaluation," *IEEE T. Automation Science and Engineering*, vol. 6, no. 2, pp. 345–361, 2009.

[18] K. Aljasem, L. Froehly, and A. S. H. Zappe, "Scanning and tunable micro-optics for endoscopic optical coherence tomography," *Journal of Microelectromechanical Systems*, vol. 20, no. 6, pp. 1462–1472, 2011.

[19] C. Clévy, M. Rakotondrabe, and N. Chaillet, *Signal measurement and estimation techniques for micro and nanotechnology*. Springer, 2011.

[20] A. Das, P. Zhang, W. Lee, D. Popa, and H. Stephanou, "Multiscale, deterministic micro-nano assembly system for construction of on-wafer microrobots," in *IEEE International Conference on Robotics and Automation*, 2007.

[21] C. Clévy, I. Lungu, K. Rabenorosoa, and P. Lutz, "Positioning accuracy characterization of assembled microscale components for micro-optical benches," *Assembly Automation*, vol. 34, pp. 69–77, 2014. [Online]. Available: https://hal.archives-ouvertes.fr/hal-00972276

[22] A. Hoover and R. Fearing, "Rapidly prototyped orthotweezers for automated microassembly," in *IEEE International Conference on Robotics and Automation*, Rome, Italy, 2007, pp. 812,819.

[23] L. Mattos and D. Caldwell, "A fast and precise micropipette positioning system based on continuous camera-robot recalibration and visual servoing," in *IEEE International Conference on Automation Science and Engineering*, Bangalore, India, 2009, pp. 609–614.

[24] R. M. Pac and D. O. Popa, "Interval analysis of kinematic errors in serial manipulators using product of exponentials formula," *IEEE Transactions on Automation Science and Engineering*, vol. 10, no. 3, pp. 525–535, 2013.

[25] P. Sandoz, R. Zeggari, L. Froehly, J. Prétet, and C. Mougin, "Position referencing in optical microscopy thanks to sample holders with out-of-focus encoded patterns," *Journal of Microscopy*, vol. 225, no. 3, pp. 293–303, 2007.

[26] N. Tan, C. Clévy, G. J. Laurent, P. Sandoz, and N. Chaillet, "Characterization and compensation of xy micropositioning robots using vision and pseudo-periodic encoded patterns," in *IEEE ICRA International Conference on Robotics and Automation*, Hong Kong, China, 2014, pp. 2819–24.

[27] R. Moddemeijer, "On the determination of the position of extrema of sampled correlators," *IEEE Transactions on Signal Processing*, vol. 39, no. 1, pp. 216–219, 1991.

[28] P. Masa, E. Franzi, and C. Urban, "Nanometric resolution absolute position encoders." *CSEM Scientific and Technical Report*, pp. 1–3, 2008.

[29] D. Boyton, "Position encoder using statistically biased pseudorandom sequence," 2003, uS Patent App. 10/399, 470.

[30] J. Galeano-Zea, P. Sandoz, E. Gaiffe, S. Launay, L. Robert, M. Jacquot, F. Hirchaud, J. Prétet, and C. Mougin, "Position-referenced microscopy for live cell culture monitoring," *Biomedical optics express*, vol. 2, pp. 1307–1318, 2011.

[31] J. Galeano-Zea, P. Sandoz, E. Gaiffe, J. Prétet, and C. Mougin, "Pseudo-Periodic Encryption of Extended 2-D Surfaces for High Accurate Recovery of any Random Zone by Vision," *International Journal of Optomechatronics*, vol. 4, no. 1, pp. 65–82, 2010.

[32] W. Khalil, S. Besnard, and P. Lemoine, "Comparison study of the geometric parameters calibration methods," *International Journal of Robotics and Automation*, vol. 15, no. 2, pp. 56–67, 2000.

[33] W. Khalil and E. Dombre, *Modeling, Identification and Control of Robots*. London: Hermes Penton Science, 2004.

[34] Y. Sun and J. M. Hollerbach, "Observability index selection for robot calibration," in *IEEE International Conference on Robotics and Automation*, 2008, pp. 831–836.

[35] T. Li, K. Sun, Y. Jin, and H. Liu, "A novel optimal calibration algorithm on a dexterous 6 dof serial robot-with the optimization of measurement poses number," in *IEEE International Conference on Robotics and Automation*, Shanghai, China, 2011, pp. 975–981.

[36] J. Hollerbach and C. Wampler, "The calibration index and taxonomy for robot kinematic calibration methods," *International Journal of Robotics Research*, vol. 15, no. 6, pp. 573–591, 1996.

[37] J. H. Borm and C. H. Menq, "Determination of optimal measurement configurations of robot calibration based on observibility measure," *International Journal of Robotics Research*, vol. 10, no. 1, pp. 51–63, 1991.

[38] M. R. Driels and U. S. Pathre, "Significance of observation strategy on the design of robot calibration experiments," *Journal of Robotic Systems*, vol. 7, no. 2, pp. 197–223, 1990.

[39] A. Nahvi and J. M. Hollerbach, "The noise amplification index for optimal pose selection in robot calibration," in *IEEE International Conference on Robotics and Automation*, Minneapolis, Minnesota, USA, 1996, pp. 647–654.